International Journal of Concrete Structures and Materials

RESEARCH

Open Access

Performance Evaluation and Microstructure Study of Pervious Concrete Prepared from Various Solid Waste Admixtures

Yi Li[1], Jiong Zhang[1*], Jie Ding[1], Feng-zhen Chen[2], Ming-zhu Liu[2], Jia Liu[1] and Zhao Hou[1]

Abstract

Solid waste materials (SWM) are commonly used in the preparation of building materials due to their structural characteristics and chemical composition. Pervious concrete (PC) is a green infrastructure material that offers advantages such as reducing surface runoff and purifying water quality, making it an important component of sponge cities. This study aims to investigate the physical properties and micro-structure of PC prepared from various SWM and determine the optimal mix proportion. In this study, three common SWM, including muck, steel slag (SS) and fly ash (FA), are used as raw materials. The chemical composition and physical properties of SWM are analyzed. A five-level and five-factor test scheme is developed using the orthogonal test method. This scheme considers the target porosity, water–cement ratio, muck content, SS content, and FA content as variables. The mechanical properties and permeability of PC, including compressive strength, porosity and permeability coefficient are evaluated. The internal structure of PC is observed using a scanning electron microscope (SEM). The results indicate that the optimal mix proportion for preparing PC is determined through efficiency coefficient method analysis: target porosity of 25%, water–cement ratio of 0.36, muck content of 10%, SS content of 10%, and FA content of 12.5%. The corresponding performance indicators of the PC sample are measured as follows: porosity of 24.67%, compressive strength of 15.78 MPa, and permeability coefficient of 2.23 mm/s. This study provides valuable insights for the rapid and flexible batching and performance optimization research of PC based on SWM.

Keywords Solid waste materials, Pervious concrete, Orthogonal test method, Microstructure

1 Introduction

With the continuous development of human society and industry, the total amount of solid waste materials (SWM) produced each year is increasing. The high cost of SWM pretreatment leads to the accumulation of SWM. Since SWM contains toxic substances, which will not only cause direct harm to the environment, but also pose risks to human health(Zhang et al., 2023), it is significant to carry out resource utilization of industrial SWM.

Researchers have devoted to exploring the possibility of recycling SWM. Gao et al. (2023) proposed a method of low-carbon and low-cost recycling muck to produce non-sintered lightweight aggregate, which has a guiding significance for the resource utilization of muck and the sustainable development of aggregate. Liu et al., (2022a, 2022b) prepared lightweight aggregates with microcrystalline diopside as the main component by using waste glass and muck as the main raw materials and the results showed that the mechanical properties of LWAs were significantly improved. Liu et al., (2022a, 2022b) studied the strength and deformation characteristics of muck-based

Journal information: ISSN 1976- 0485 / eISSN 2234-1315.

*Correspondence:
Jiong Zhang
jiongzhang@sdu.edu.cn
[1] School of Civil Engineering, Shandong University, Jingshi Road 17922, Jinan 250061, China
[2] Shandong Dayu Water Construction Group Co, LTD, Jinan 250061, China

foamed concrete which added muck to replace part of the cement. As a solid waste produced in the process of crude steel refining, SS is not only a good mineral admixture for concrete (Wang et al., 2013),but also can be used as aggregate of cement materials (Shen et al., 2009).Basavana Gowda et al. (2023) used steel slag to completely replace ordinary Portland cement as the binder for the preparation of alkali activated slag based PC. Shen et al. (2020) optimized the preparation process of PC by utilizing carbonated steel grinding slag powder as a binder and crushed steel slag as an aggregate. Teymouri et al. (2023) examined the engineering properties of iron slag pervious concrete and its effectiveness in water purification. The results revealed that PC containing 15% SS demonstrated superior performance in reducing surface runoff pollution. Zhang et al. (2020) investigated the impact of binder–aggregate ratio and various binders on the performance and micro-structure of PC using SS as aggregate. FA is used as a cement substitute in blended cement or concrete and is valued for its potential advantages, including greater structural strength, cost efficiency, and environmental sustainability (Shukla et al., 2023). In the study conducted by Nazeer et al. (2023), FA and silica fume were utilized in partial replacement of cement for the production of peritoneal concrete. Sherwani et al. (2021) cold bonded FA and Portland cement at the ratio of 9:1 to obtain artificial cold bonded fly ash aggregate (AFA), and prepared PC by replacing natural aggregate with AFA. Valerie López-Carrasquill et al. (2017) optimized the FA used for preparing PC by adding three kinds of nanomaterials, respectively. The results showed that PC_{NS} (nano-SiO_2) and PC_{NI} (nano-iron) had better performance.

The strength of PC is mainly derived from aggregate performance, paste performance, and the bond strength of the paste (Zhong & Wille, 2015). When PC undergoes compression damage, its well-developed pore structure causes PC to exhibit different damage modes at the meso-level, including aggregate failure, paste failure, and interfacial transition failure (Liao et al., 2023). There are various forms and modes of degradation that may occur during compressive strength testing of PC (Adresi et al., 2023). S. Nassiri et al. (2017) recorded for each tested specimen during the compression test. Moreover, there are three additional failure types: columnar cracks, shear with the cone, and side fracture on both ends. Han et al. (2022) proposed a new method based on the boundary effect model (BEM) to determine the fracture characteristics of PC, while incorporating the micro-structure of the material and the geometry of the specimen in the form of virtual cracks. The results show that the strength of PC is strengthened with the increase of aggregate particle size. Cui et al.(2024) conducted the numerical test model of the dynamic hollow cylinder on the sub-grade soil, and the influence of principal stress rotation on the macro–micro evolution of dynamic characteristics was analyzed. In addition, weak aggregate–paste bond, allowed cracks to develop, which caused poor aggregate–paste binding and increased porosity (Brasileiro et al., 2024). Besides the damage investigation of PC to lab tests, it is more practical to study the scattering of the fracture energy in the micro-structure of concrete. Hoang-Quan Nguyen et al.(2022) used the numerical model based on the finite element methods and the phase field theory to evaluate the flexural damage behavior and energy of PC. The obtained results demonstrated the important role of pore structure, which plays as a key control parameter in the mechanical response of PC. The digital image correlation (DIC) technique is used to crack propagation and crack opening profiles in the fracture response of concrete beams are evaluated as well (Chakraborty and V. L. Subramaniam, 2023).

Considering the future trend of utilizing SWM for building materials, this paper investigates the use of three types of SWM, namely muck, SS, and FA, in the preparation of PC. Previous research has extensively utilized SS and FA in the production of PC, however, there is a noticeable gap in studies focusing on incorporating muck into the mix. This study aims to assess the feasibility of preparing PC using three common types of SWM—muck, SS, and FA. The findings of this research hold significant importance for enhancing the utilization of SWM within the PC industry. Furthermore, the chemical reaction mechanism of SWM preparation of PC was analyzed by XRD and SEM images in this study. In addition, the study introduces the novel application of the efficiency coefficient method to comprehensively evaluate the overall performance of PC. Through a detailed analysis of permeability coefficient and compressive strength, the study determines the optimal mix ratio for PC. In general, this study employs the orthogonal test method to examine the effects of target porosity, water–cement ratio, muck content, SS content, and FA content on the physical properties of PC, including compressive strength, porosity, and permeability coefficient. Additionally, the optimal mix proportion is determined based on the efficiency coefficient method and microscopic observation of the PC's micro-structure, ensuring practical applicability in engineering. The experimental data obtained from this study offer reliable guidance for the application of PC prepared with SWM, and the results hold significant importance

Table 1 Physical and chemical properties of muck

PH	ω/%	Unit weight g/cm^3	Porosity	Liquid limit/%	Plastic limit/%	Liquid index	Plasticity index	Organic matter content/g/kg
7.62	> 100	0.89	5.956	31.28	17.57	8.13	28.4	189

Table 2 Particle composition of muck

Particle composition					
Particle size (mm)					
> 2	2–0.5	0.5–0.25	0.25–0.075	0.075–0.002	< 0.002
%	%	%	%	%	%
0.0	1.4	1.1	23.2	65.4	8.9

for promoting resource sustainability and environmental protection.

2 Experimental Investigation

2.1 Experimental Materials

The muck used in this study was obtained from the water quality improvement project of Meicheng Park in Jinan City, Shandong Province, China. It was shallowly buried and had a high water content. The cement used in the experiment was P.O 42.5 ordinary Portland cement, supplied by Jiuqi Building Materials Co., Ltd, China. Grade I SS and grade I FA were provided by Borun Materials Co., Ltd. in Gongyi City, Henan Province, China. The test used coarse aggregate, which was gravel with a particle size of 6-9 mm, and fine aggregate, which was medium sand with a particle size of 0.25–0.5 mm. A polycarboxylic acid superplasticizer was used as the water reducing agent, with a dosage of 0.7% of the total mass of cementitious materials. Table 1 to Table 4 provide information on the physical and mechanical properties, particle composition of the muck, mineral parameter composition, and main chemical composition of the tested raw materials.

Based on the measurements presented in Table 1, the muck exhibits high moisture content, low strength, high compressibility, and low shear strength. According to Table 2, it can be observed that more than 85% of the muck particles fall within the range of 0.002–0.075 mm, with 8.9% of the particles measuring less than 0.002 mm. Referring to ASTM D422-63, the muck particles consist primarily of sandy soil, with a small portion being cohesive soil. Analysis of the chemical compositions of the three solid waste admixtures in Table 3 reveals a significant presence of active SiO_2 and Al_2O_3 in the muck and FA. Table 4 presents the results of the mineral composition analysis of three types of SWM using XRD. The analysis reveals that muck primarily consists of quartz, plagioclase, and $CaCO_3$, whereas SS and FA contain a significant amount of amorphous minerals. It is important to note that, unlike the mineral composition of cement, the three types of SWM do not contain a substantial quantity of C_2S or C_3S. Instead, these two substances are not detected in muck and FA, and only a small amount of C_2S is detected in SS.

The mechanism of cement curing encompasses various processes, including the hydration reaction of cement itself, the cementation, filling, and skeleton effects of the

Table 3 The main chemical composition of solid waste admixture

Species/composition	SiO_2/%	CaO/%	Al_2O_3/%	Fe_2O_3/%	MgO/%	SO_3/%
Cement	18.99	60.42	8.26	4.03	/	2.51
Muck	49.62	17.86	13.24	7.96	3	2.14
SS	12.60	46.85	6.07	12.61	5.63	/
FA	45.10	5.60	24.20	0.85	/	2.10

Table 4 Mineral composition of solid waste admixture

Species/mineral composition	C_3S/%	C_2S/%	Amorphous substance/%	Quartz/%	FeO/%	Plagioclase/%	$CaCO_3$/%	Al_2SiO_4/%
Muck	/	/	/	44.70	/	17.00	15.40	/
SS	/	14.30	62.20	1.90	15.70	/	/	/
FA	/	/	69.40	8.40	/	/	/	22.20

hydration products, the ion exchange between the hydration product $Ca(OH)_2$ and clay minerals, the volcanic ash effect, and the carbonation effect. The hydration reaction of cement involves two main parts: first, the hydration reaction of the mineral phase of cement clinker itself, and then the hydration reaction of the hydration products of cement clinker and the active components in solid waste materials, such as SiO_2 and Al_2O_3. Among the hydration reactions of cement clinker minerals, C_3S hydration is the primary component, and its specific hydration reaction is shown in formula (1):

$$3CaO \cdot SiO_2 + nH_2O \rightarrow xCaO \cdot SiO_2 \cdot yH_2O + (3-x)Ca(OH)_2, \tag{1}$$

where n represents the amount of water involved in the hydration reaction, x and y represent the CaO/SiO_2 molecular ratio and H_2O/SiO_2 molecular ratio of C-S–H, respectively.

In the alkaline environment generated by the cement hydration reaction, Ca^{2+} reacts with part of SiO_2 and Al_2O_3 to form stable crystalline minerals C-A-H and C-S–H that are insoluble in water (Liu et al., 2023, Zhu et al., 2023). The use of SS as an admixture in PC not only enhances its hydration through the heat generated by cement, but also benefits from the alkali produced during cement hydration (Zhao et al., 2023). During the initial stage of the reaction, a significant amount of CaO in SS reacts with water to form $Ca(OH)_2$. Simultaneously, C_2S in SS undergoes a hydration reaction to produce C-S–H, as depicted in formula (2):

$$\begin{aligned} &CaO + H_2O \rightarrow Ca(OH)_2 2CaO \cdot SiO_2 + nH_2O \\ &\rightarrow xCaO \cdot SiO_2 \cdot yH_2O + (2-x)Ca(OH)_2, \end{aligned} \tag{2}$$

where n represents the amount of water involved in the hydration reaction, x and y represent the CaO/SiO_2 molecular ratio and H_2O/SiO_2 molecular ratio of C-S–H, respectively. The difference between SS and cement hydration reaction is that C_2S in SS leads to the lower hydration rate in the initial stage.

The significant amount of $Ca(OH)_2$ produced through the hydration reaction of cement and SS establishes an alkaline environment within the reaction system. In this alkaline environment, muck and FA dissolve, leading to the formation of $[SiO_4]^{4-}$ and $[AlO_4]^{5-}$. These ions then react with OH^- to create C-S–H and C-A-H. As a result of consuming a substantial quantity of OH^-, durable and compact pozzolanic reaction products are formed, ultimately enhancing the strength of PC. The chemical formula of the reaction between the active component in SWM and $Ca(OH)_2$ produced by the hydration reaction cement is shown in formula (3):

$$\begin{aligned} &SiO_2 + xCa(OH)_2 + mH_2O \rightarrow xCaO \cdot SiO_2 \cdot mH_2O \\ &Al_2O_3 + yCa(OH)_2 + nH_2O \rightarrow yCaO \cdot Al_2O_3 \cdot nH_2O, \end{aligned} \tag{3}$$

where x and y represent the CaO/SiO_2 molecular ratio and CaO/Al_2O_3 molecular ratio of C-S–H and C-A-H, respectively, m and n represent the amount of water involved in the hydration reaction which means the H_2O/SiO_2 molecular ratio.

Therefore, not only can the hydration reaction of cement itself provide strength for PC, but also the reaction of active substances in SWM and cement hydration products can also form a structural whole with certain strength. In order to obtain the optimal mixture ratio scheme and appropriate mixing amount for the preparation of PC based on SWM, different mixture ratio schemes composed of step control variables need to be designed.

2.2 Experimental Methods

- Muck Pretreatment

Due to high moisture content and a large amount of impurities, fresh muck samples cannot be directly used as experimental raw materials, the sampling site is shown in Fig. 1.

The freshly collected muck samples from the field are initially laid out and dried in order to eliminate moisture (a). Subsequently, the initial grinding and impurity removal takes place (b). The pretreated muck block is then inserted into the solid sample crusher for crushing and grinding (c). Following a 3-min grinding process, the muck particles are filtered through a screen, resulting in the acquisition of fine particles ranging from 0.050 mm to 0.075 mm (d). These fine muck particles serve as the raw materials for testing purposes. The pretreatment process

Fig. 1 Environment of muck sampling site

Fig. 2 Muck pretreatment process

is shown in Fig. 2. A, b, c and d in Fig. 2 represent the four steps of the muck pretreatment process respectively.

- Pervious Concrete Mix Design Method

When designing the mix proportion of PC, two important performance indicators are the permeability and strength after molding (Hari and K. M., 2024). The permeability of PC is mainly affected by the porosity (E et al., 2021; Pereira Da Costa et al., 2021), while the strength is influenced by the strength of the cement slurry and the bonding force of the aggregate (Chockalingam et al., 2023; Claudino et al., 2022; He et al., 2023). In this study, five crucial control parameters were selected for the mix proportion design: target porosity, water–cement ratio, muck content, SS content, and FA content:

(1) Target porosity: The porosity of PC should be greater than 10%, so the mix ratio design of this test set a total of 5 target porosity, respectively, 10%, 15%, 20%, 25% and 30%.
(2) Water–cement ratio: The water–cement ratio is an important factor affecting the micro-structure of cement slurry (Dhemla et al., 2023), and five kinds of water–cement ratio are designed in this experiment, which are 0.36, 0.38, 0.40, 0.42 and 0.44, respectively.
(3) Muck content: This study chooses five different muck contents, namely 5%, 7.5%, 10%, 12.5%, and 15%, to represent the mass fraction of muck in the cementitious material.
(4) SS content: Based on previous research, this study selects five different SS contents, namely 5%, 10%, 15%, 20% and 25% (Lang et al., 2019), representing the mass fraction of SS in the cementitious material.
(5) FA content: Bright Singh et al. (Bright Singh et al., 2023a) have conducted previous research and this study selects five different FA contents, namely 5%, 7.5%, 10%, 12.5%, and 15%, to represent the mass fraction of FA in the cementitious material.

According to the "Technical specification for pervious cement concrete pavement" (CJJ/T135-2009) (Ministry Of Housing And Urban–Rural Development, 2009), the design of PC mix is calculated by volume method, and its strength is determined by subsequent tests. The basic calculation principle of volume method is shown in formula (4):

$$\frac{M_G}{\rho_G} + \frac{M_C}{\rho_C} + \frac{M_W}{\rho_W} + \frac{M_Z}{\rho_Z} + \frac{M_J}{\rho_J} + P = 1, \tag{4}$$

where M_G represents the mass of aggregate per m^3, M_C represents the mass of concrete per m^3, M_W represents the mass of water per m^3, M_Z represents the mass of SWM per m^3 and M_J represents the mass of admixture per m^3. Additionally, we have ρ_G, ρ_C, ρ_W, ρ_Z, and ρ_J representing the apparent density of aggregate, concrete, water, SWM, and admixture, respectively. P represents the target porosity. It is important to note that there are three types of SWM used in this test, namely muck, SS, and FA. During the calculation process of mix proportion design, we calculate the mass of each type of mineral admixture per m^3 of mixture separately.

To address the problem of multi-factor and multi-level optimization design, the widely adopted approach is the orthogonal test method. This method adheres to mathematical principles and identifies factors and levels with orthogonal properties from a vast array of test factors. As a result, it efficiently minimizes the number of tests required while yielding excellent results (Chen et al., 2023). The selected factors included target porosity, water–cement ratio, muck content, SS content, and FA content. Five different levels were chosen for each of these factors, resulting in a total of 25 test cases to study their effects. To determine performance, 9 samples were made for each test case. The horizontal factors can be seen in Table 5. The first row in Table 5 represents the grade level in the orthogonal test. In this study, the orthogonal test adopted includes 5 different grade levels for each factor, which are different target porosity, water–cement ratio, and SWM content.

- Method for Determination of Pervious Coefficient of Pervious Concrete

One major flaw in the current method of measuring the PC permeability coefficient is the issue of side wall leakage in the PC specimen during the measurement process. The PC specimen, prepared in the laboratory using a mold, has a rough surface and large pore diameter. These open pores on the side surface of the specimen create pathways between the side wall of the sleeve and the specimen's side surface. Due to the significantly lower resistance of these open channels compared to the internal permeable pores of the PC, a majority of the water tends to flow out through these channels. As a result, the measured permeability coefficient in the test is higher than the actual value.

Table 5 Different factors of orthogonal test correspond to levels

Factor/level	I	II	III	IV	V
Target porosity/%	10	15	20	25	30
Water–cement ratio	0.36	0.38	0.40	0.42	0.44
Muck dosage(ω) /%	2.5	5	7.5	10	12.5
SS dosage(ω) /%	5	10	15	20	25
FA dosage(ω) /%	2.5	5	7.5	10	12.5

In order to overcome the limitations that the measured permeability coefficient is too large due to sidewall leakage in traditional measurement methods, our research group has developed an improved permeability testing method (Cui et al., 2015). This method involves the use of a specially designed device to accurately measure the permeability coefficient of PC, which is a composite side wall structure consisting of Vaseline, a flexible rubber pad, and a Plexiglass sleeve. The device effectively prevents sidewall leakage, resulting in improved testing accuracy of the permeability coefficient. Additionally, the device is simple to operate and cost-effective. The specific test device diagram is shown in Fig. 3.

- Method for Determination of True Porosity of Pervious Concrete

Based on previous research and laboratory equipment conditions, the wire method was selected in this study to determine the true porosity of PC (Akkaya & Çağatay, 2021; Bright Singh et al., 2023b). The process of investigating the true porosity is illustrated in Fig. 4. The main devices used in the test to measure the true porosity include spring tension machines, ovens, electronic scale and ropes. The cured PC specimen was placed in an oven and maintained at a constant temperature for 24 h. Subsequently, the dry mass of the specimen (m_1) was measured using an electronic scale. The spring tension meter served as a simple hydrostatic balance in the test. By attaching the upper end of the tension meter and securing the PC specimen on the lower end with a thin cord, the specimen was gradually fully immersed in water. The tension meter value was recorded when no bubbles were observed emanating from the specimen, and the mass of the test piece in water (m_2) was calculated.

The porosity of the sample is calculated by the difference between its dry mass and its mass in water. The calculation of porosity is shown in formula (5):

$$P = \left(1 - \frac{m_1 - m_2}{V}\right) \times 100\%, \tag{5}$$

where P is porosity, m_1 is the dry mass of the specimen, m_2 is the mass of the specimen in water, and V is the volume of the specimen.

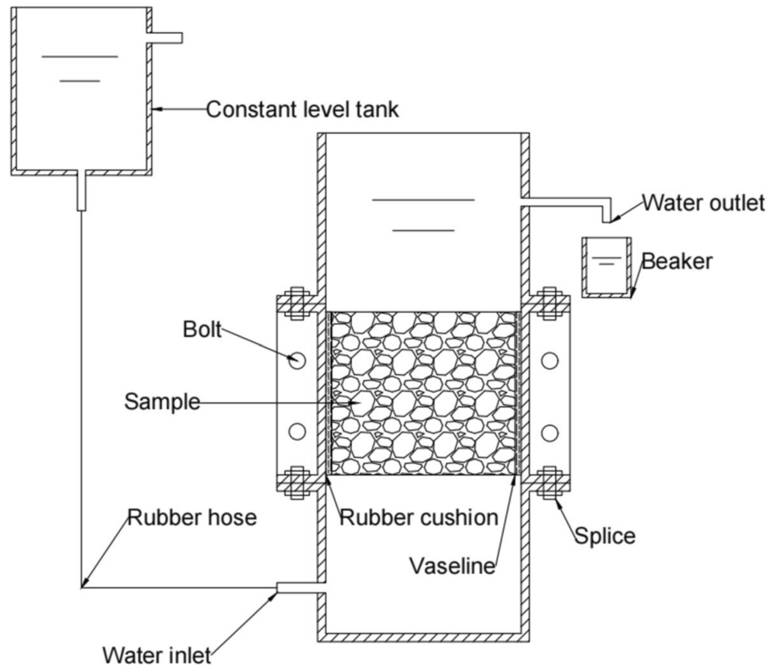

Fig. 3 Schematic diagram of permeability coefficient measuring device

Fig. 4 Devices for measuring true porosity

Fig. 5 Devices for measuring compressive strength

- Method For Determination of Compressive Strength of Pervious Concrete

Following the Chinese standard GB/T 50010–2010(China, 2010), the compression experiment was carried out using the 650-kN electric stress direct shear apparatus as shown in Fig. 5, and the loading speed was controlled at 0.8–1.0Mpa/s. The maximum load of the specimen under pressure until yield was recorded. The measured value of the compressive strength of a group of specimens was the average value of the compressive strength of three specimens. The calculation of compressive strength is shown in formula (6):

$$f = \frac{F}{A}, \tag{6}$$

where F represents maximum load, A represents the compression area, and f is the compressive strength of specimen.

3 Results and Discussion

Based on the orthogonal test method adopted in this study, the range analysis method is used in data analysis (Li et al., 2024). The range analysis of data can visually obtain the degree of influence of various factors on the physical strength of PC samples.

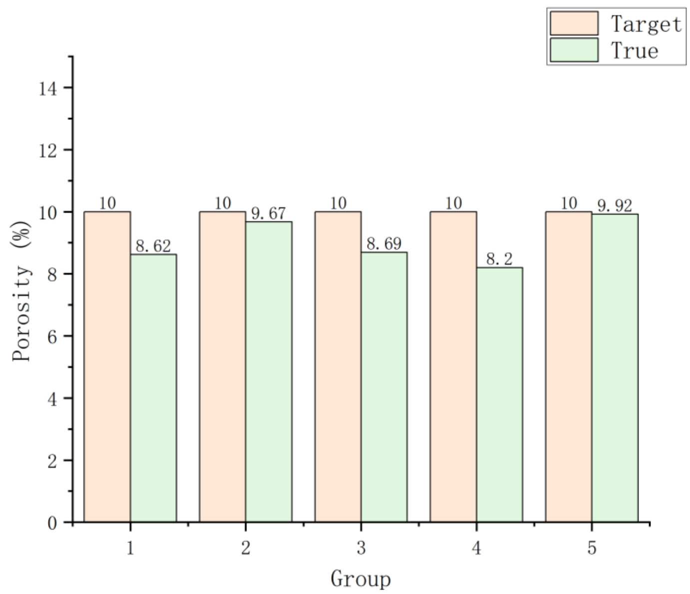

(a) The test group with a target porosity of 10%

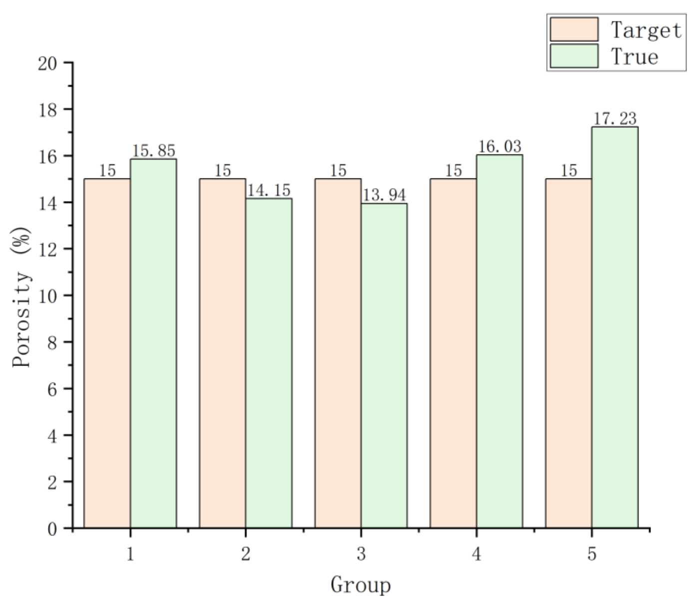

(b) The test group with a target porosity of 15%

Fig. 6 Comparison of true porosity and target porosity.

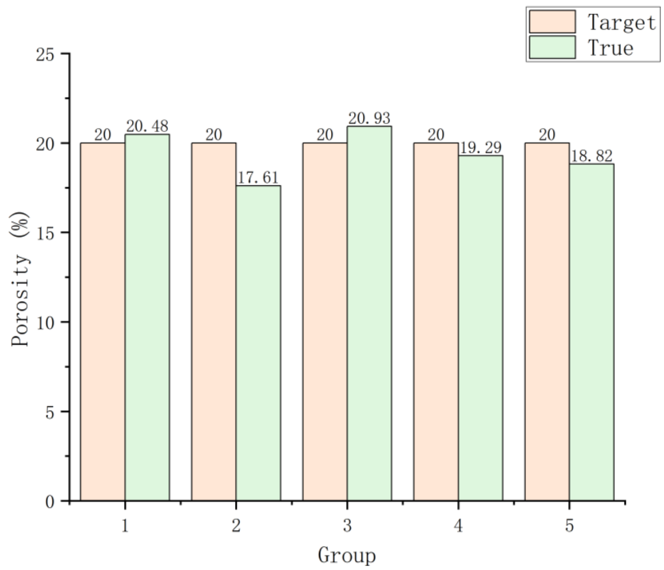

(c) The test group with a target porosity of 20%

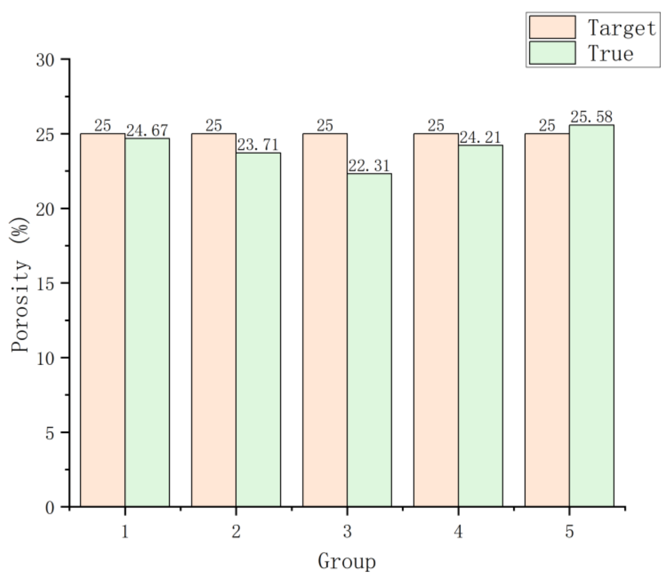

(d) The test group with a target porosity of 25%

Fig. 6 continued

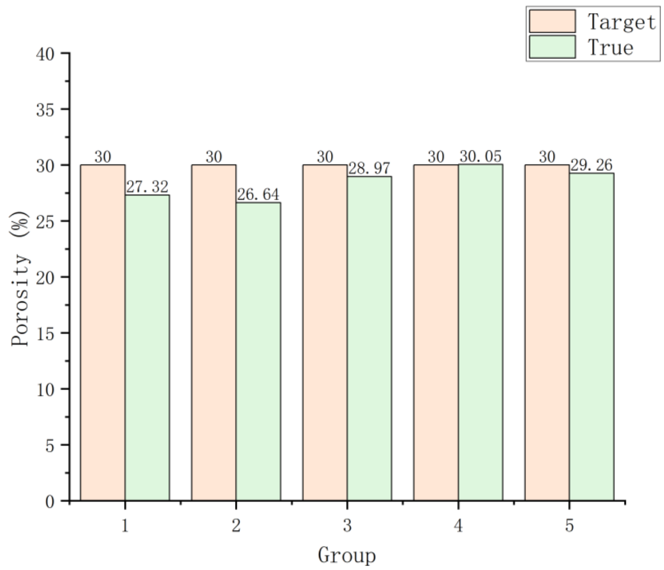

(e) The test group with a target porosity of 30%

Fig. 6 continued

3.1 Analysis of True Porosity

The porosity measured during the test was compared to the target porosity, and the results are shown in Fig. 6. The small difference between the true porosity and the target porosity indicates that the proposed mix proportion scheme is effective in controlling porosity. In Fig. 6, "target" represents the schematic diagram of target porosity, and "true" represents the schematic diagram of the measured porosity.

Fig 6 also reveals that not all concrete samples meet the requirements under the same target porosity. To assess the extent to which the porosity of the samples meets the requirements for different target porosity conditions, the mean square error calculation method is used to quantify the dispersion. The calculation shows that the minimum mean square error is 0.66 when the target porosity is 10%, while the maximum mean square error is 1.26 when the target porosity is 30%. This suggests that for the PC sample, it becomes more challenging to control the true porosity as the target porosity increases.

3.2 Analysis of Compressive Strength

In orthogonal testing, the range analysis method is commonly employed to analyze test results. By conducting range analysis on the test data, the impact of different factors on the results can be visually organized. Each factor's level change affects the test results differently, and range analysis helps in determining the primary and secondary effects of these changes. A larger range difference signifies a greater influence of the factor's level change on the test index, while a smaller range indicates a lesser impact on the test index. The range analysis method was employed to analyze the measurement results of PC's compressive strength. By calculation, the factors affecting compressive strength, in order of significance, are target porosity, water–cement ratio, muck content, FA content, and SS content. Fig. 7 visually illustrates the variations in average compressive strength of PC under different levels of these factors. The "R" in Fig. 7 and the corresponding values represent the range between the different indicators.

As shown in Fig. 7a, the compressive strength of PC decreases significantly as the target porosity increases. PC has a skeleton pore structure (Li et al., 2023), and increasing the target porosity results in more internal pores, reducing the structural density and compressive strength. Fig. 7b demonstrates that the compressive strength of PC initially increases and then decreases with the water–cement ratio. A smaller water–cement ratio leads to an increase in cement dosage for the same target porosity. However, this can prevent the full wrapping of aggregates by the cementitious material, reducing the strength of PC. Conversely, a larger water–cement ratio decreases the cement content, also leading to a decrease in strength (Oyunbileg et al., 2023; Yao et al., 2022).

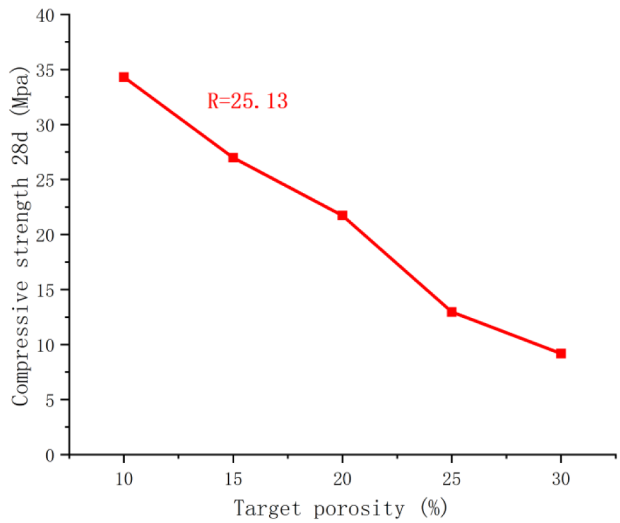

(a) Compressive strength under different target porosity

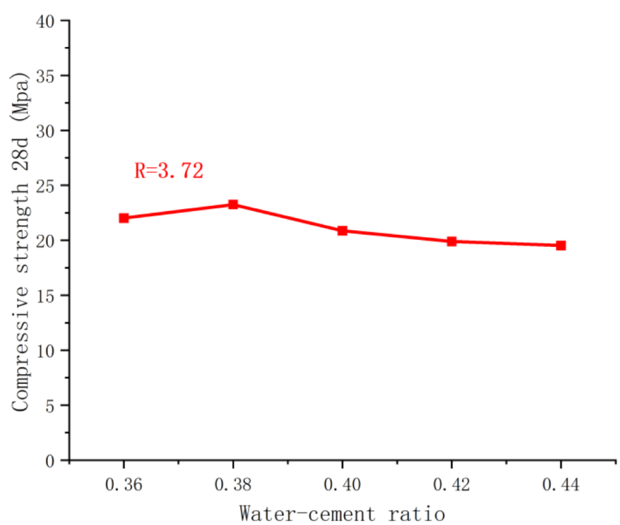

(b) Compressive strength under different water-cement ratio

Fig. 7 The effect curve of compressive strength of PC.

Fig. 7c and e shows that the compressive strength of PC follows a trend of increasing first and then decreasing with the dosage of muck and FA. The addition of appropriate muck and FA can react with $Ca(OH)_2$ to produce high-strength C-S–H and C-A-H due to their chemical composition. However, excessive dosage of muck and FA cannot fully utilize the activity of the material, resulting in a decrease in cement dosage and compressive strength of PC. Among the three types of SWM, muck and FA enhance the strength of PC when used in a dosage of less than 10%. Increasing the dosage of muck and FA from 2.5% to 10% leads to an increase in compressive strength by 15.41% and 9.92%, respectively.

According to the results shown in Fig. 7d, the compressive strength of PC decreases as the dosage of SS increases. SS, as a mineral admixture, can enhance the

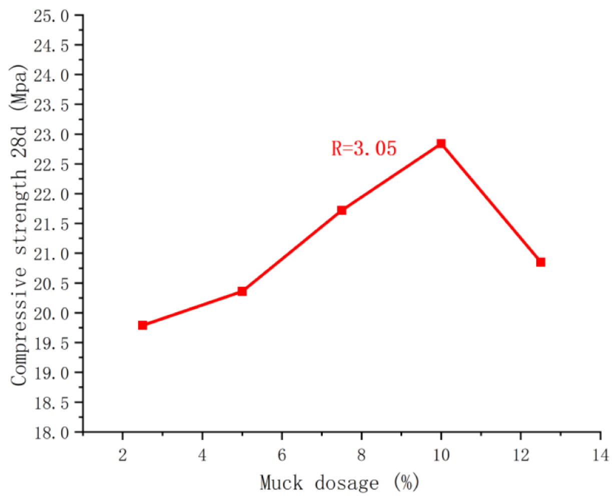

(c) Compressive strength under different muck dosage

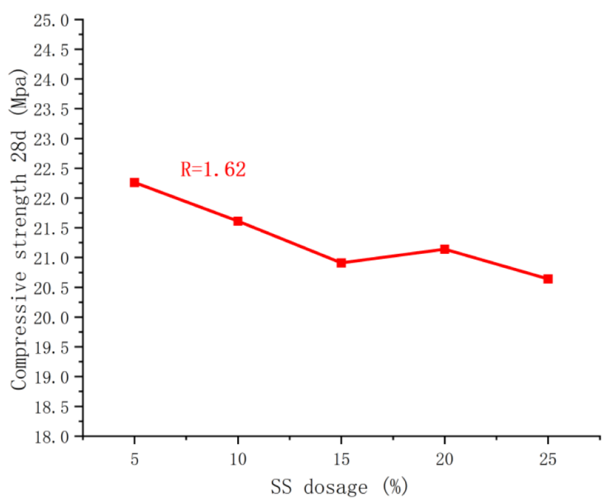

(d) Compressive strength under different SS dosage

Fig. 7 continued

performance of PC. However, it is challenging to fully activate the activity of SS when various SWM are present. Moreover, increasing the dosage of SS can negatively impact the cohesion of cement paste, thereby affecting the strength development.

3.3 Analysis of Permeability Coefficient

Similar to the analysis of compressive strength of permeable concrete, the range analysis method was used to analyze the permeability coefficient of PC. Overall, the factors affecting the permeability coefficient in descending order are target porosity, water–cement ratio, SS dosage, FA dosage, and muck dosage. Additionally, Fig. 8 visually illustrates the variations in the average permeability coefficient of PC across different levels of the various factors. The "R" in Fig. 8 and the corresponding values represent the range between the different indicators.

As depicted in Fig. 8a, the permeability coefficient of PC increases as the target porosity increases. This

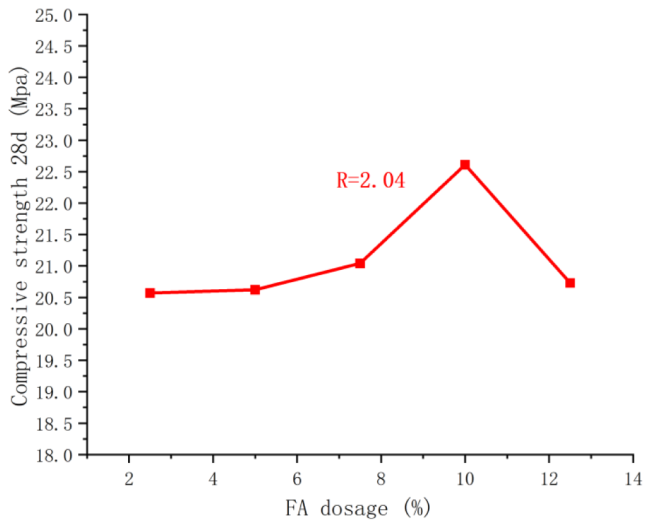

(e) Compressive strength under different FA dosage

Fig. 7 continued

increase in target porosity inevitably results in the formation of more internal pores in concrete, thereby enhancing the permeability of PC. On the other hand, Fig. 8b demonstrates that the permeability coefficient of PC decreases with an increase in the water–cement ratio. A lower water–cement ratio leads to incomplete coverage of the aggregate by the cement slurry, causing an increase in pores. Although this may not be beneficial for the strength of PC, it improves its permeability. Conversely, a higher water–cement ratio leads to the excess cement slurry filling the pores, which negatively affects the permeability of PC.

According to Fig. 8c, d, and e, the permeability coefficient of PC generally increases initially and then decreases as the dosage of muck, SS, and FA increases. The optimal amount of SWM can create a strong skeleton structure by reacting with the cement, which not only meets the mechanical property requirements of PC, but also enhances the porosity of the PC structure and improves permeability. However, excessive SWM dosage can lead to unreacted surplus SWM blocking the pores, thereby negatively affecting PC permeability. When the muck dosage increases from 2.5% to 5%, the permeability coefficient increases by 5.56%. Similarly, increasing the SS dosage from 15 to 20% results in a 39.25% increase in the permeability coefficient. Likewise, increasing the FA dosage from 2.5% to 7.5% leads to a 38.26% increase in the permeability coefficient.

3.4 Comprehensive Performance Analysis

The above two sections analyze the extent and overall trend of various factors' influence on the compressive strength and permeability coefficient of PC. However, to obtain an optimal mix proportion scheme for preparing PC using SWM, a method is required to conduct a comprehensive analysis of the test data. The efficiency coefficient method was employed to normalize each index and determine the efficiency coefficient of the corresponding index. Subsequently, the total efficiency coefficient was calculated based on the efficiency coefficient of each index. A higher total efficiency coefficient indicates a better comprehensive performance of the mix ratio of the restructured test. The normalization calculation of each index and the calculation of the total efficiency coefficient are presented in formula (7):

$$\begin{gathered} d_{ji} = \frac{T_{ji}}{T_{\max}} \\ d_j = \sqrt[n]{(d_{j1} \times d_{j2} \times \ldots \times d_{jn})}, \end{gathered} \tag{7}$$

where d_{ji} is the efficacy coefficient of the ith index in the jth case of tests; T_{ji} is the measured value of the ith index in the jth case of tests; T_{max} is the measured maximum value of the ith index in the 25 cases of tests; d_j is the total efficacy coefficient of the jth case of tests; n is the number of evaluation indexes.

This study comprehensively analyzed the compressive strength and permeability coefficient obtained from the orthogonal test using the efficiency coefficient method.

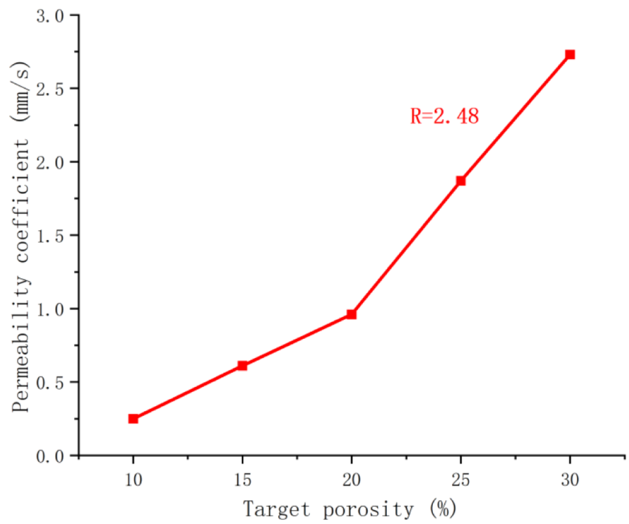

(a) Permeability coefficient under different target porosity

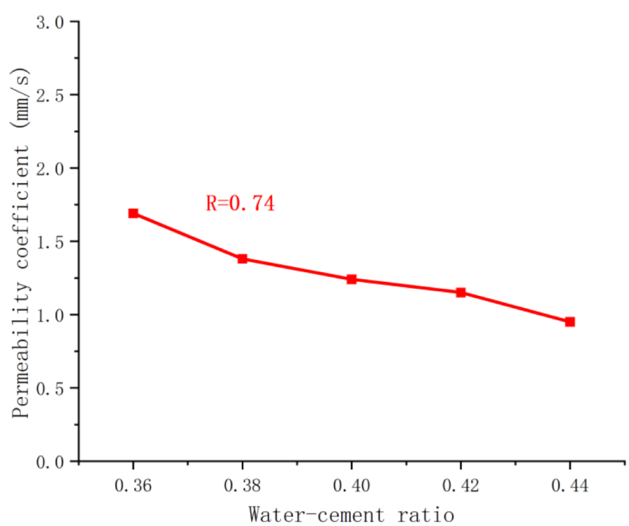

(b) Permeability coefficient under different water-cement ratio

Fig. 8 The effect curve of permeability coefficient of PC.

The specific calculation results are presented in Table 6 as follows.

Considering that the compressive strength of PC in practical engineering application is required to be no less than 15 Mpa, the 16th case of tests is selected as the design scheme of PC mix ratio with the best comprehensive performance in this test scheme. The corresponding measured performance indexes of PC are true porosity of 24.67%, compressive strength of 15.78Mpa, permeability coefficient of 2.23 mm/s.

3.5 Study on Micro-Structure of Pervious Concrete

- Study on Micro-Structure of Interface Transition Zone (ITZ) in Pervious Concrete

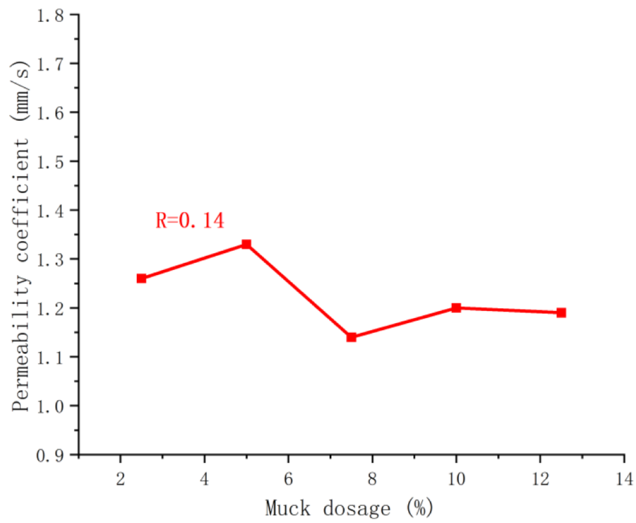

(c) Permeability coefficient under different muck dosage

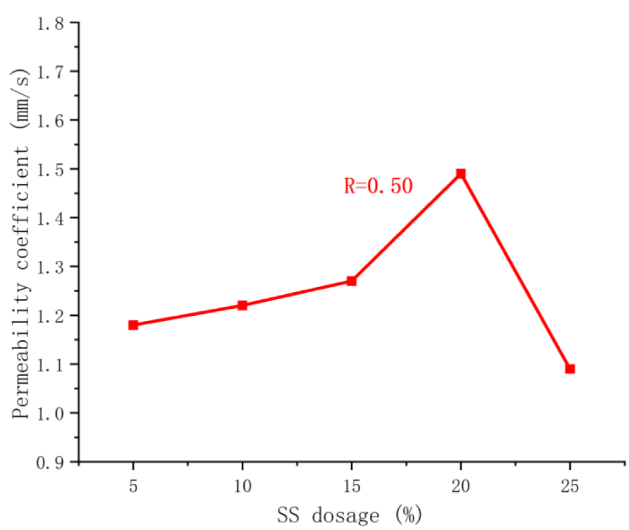

(d) Permeability coefficient under different SS dosage

Fig. 8 continued

The interfacial transition zone (ITZ) is widely regarded as the mechanical vulnerability of concrete. Similarly, ITZ in PC exhibits distinct structural and property differences compared to the cement body structure (Chockalingam et al., 2023; Oyunbileg et al., 2023; Ren et al., 2024). The quality of this transition zone directly impacts the strength and durability of PC (Kishore and Tomar, 2023).

Fig. 9a, b and c displays SEM images of the ITZ of various PC samples examined under the scanning electron microscope (SEM) in this study. By analyzing Fig. 9a, b, and c, it becomes evident that there is a significant presence of C-S–H gels near the aggregate in the ITZ. This presence is advantageous for the development of the strength of PC. The formation of C-S–H through the chemical reaction between the cement slurry and the

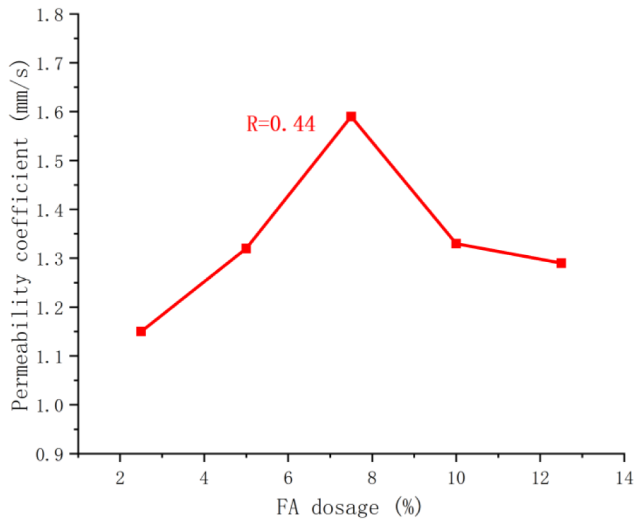

(e) Permeability coefficient under different FA dosage

Fig. 8 continued

aggregate leads to a reduction in the content of $Ca(OH)_2$ in the transition zone. Larger $Ca(OH)_2$ crystals have poor bonding ability, not only because of their small surface area, but also because their tendency to form oriented structures tends to be the first place to be damaged (Liu et al., 2018). The chemical reaction between the cement slurry and the aggregate leads to the formation of C-S–H, which reduces the content of $Ca(OH)_2$ in the ITZ. Larger $Ca(OH)_2$ crystals have poor bonding ability due to their small surface area and tendency to form oriented structures, making them susceptible to damage (Liu et al., 2018). The prolonged hydration period of PC, resulting from the hydration reactions of cement and secondary reactions of SWM, strengthens the ITZ by generating hydration products. As the strength of the PC improves, the bond between the aggregate becomes tighter, leading to a denser ITZ. It is worth noting that Fig. 9 (a) and (b) still shows the presence of partially layered $Ca(OH)_2$. This occurrence arises when the cement dosage is high and the SWM dosage is low, preventing the complete consumption of $Ca(OH)_2$ generated by the cement hydration reaction. Consequently, this situation hampers the strength development of the ITZ. However, in Fig. 9c, a substantial amount of C-S–H is observed, indicating a more comprehensive reaction between SWM and $Ca(OH)_2$ in the optimal mix proportion scheme. Hence, the appropriate dosage of SWM is crucial for enhancing the ITZ strength of PC. The panels in Fig. 9 represent the identification of different products.

The utilization of SWM in the preparation of PC has a positive impact on the strength of the ITZ. This $Ca(OH)_2$ has been found to have a detrimental effect on the strength development of ITZ. However, the active substances present in SWM can react with $Ca(OH)_2$, leading to an improvement in the strength of the PC's ITZ.

- Study on Micro-structure Morphology of Pervious Concrete

The correlation between micro-structure and properties is of paramount significance in contemporary materials science. PC possesses a micro-structure distinguished by its elevated heterogeneity and complexity. A comprehensive comprehension of both the micro-structure and properties of each constituent within PC, coupled with their interdependence, can facilitate meticulous control over concrete performance (Shen et al., 2021). The visualization of the observations is depicted in Fig. 10. The

Table 6 Calculation of efficiency coefficient of PC

Case	Compressive strength/Mpa	d_{j1}	Permeability coefficient/mm/s	d_{j2}	d_j
1	35.64	1	0.30	0.07	0.26
2	34.14	0.96	0.28	0.07	0.26
3	35.46	0.99	0.25	0.06	0.24
4	34.76	0.98	0.26	0.06	0.24
5	31.53	0.88	0.14	0.03	0.16
6	28.36	0.80	0.76	0.19	0.39
7	30.52	0.86	0.68	0.17	0.38
8	26.88	0.75	0.69	0.17	0.36
9	27.21	0.76	0.43	0.11	0.29
10	21.93	0.62	0.47	0.12	0.27
11	21.10	0.59	1.13	0.28	0.41
12	27.00	0.76	1.05	0.26	0.44
13	23.76	0.67	0.99	0.25	0.41
14	18.45	0.52	0.78	0.19	0.31
15	20.35	0.57	0.85	0.21	0.35
16	15.78	0.44	2.23	0.56	0.50
17	12.51	0.35	1.78	0.44	0.39
18	10.86	0.30	1.66	0.41	0.35
19	11.59	0.33	2.16	0.54	0.42
20	14.07	0.39	1.52	0.38	0.39
21	9.24	0.26	4.01	1	0.51
22	12.08	0.34	3.11	0.78	0.51
23	7.36	0.21	2.62	0.65	0.37
24	7.45	0.21	2.14	0.53	0.33
25	9.77	0.27	1.76	0.44	0.34

digital panel at the bottom of Fig. 10 represents the parameters of an electron microscope.

Specific analysis of each set of images shows that there are some SWM particles with smooth surfaces, indicating that these large particle size SWM particles are basically not involved in the reaction, and the large particle size SWM particles without reaction will be filled in the hydration product or located on its surface, reducing the water permeability of the PC. Fig. 10b and Fig. 10c illustrate that the products of cement hydration and secondary reactions primarily consist of mesh-like and coral-like hydrated calcium silicate gel (C-S–H), dendritic ettringite (AFt), and layered $Ca(OH)_2$. The mechanical properties of the samples show a decreasing trend in compressive strength from Fig. 10a to Fig. 10c. Upon observing the micro-structure morphology, it becomes evident that the change in density of the cement matrix in the SEM image follows a similar trend as the compressive strength. However, it is challenging to differentiate the specific regions of hydration product. The hydration products in PC were qualitatively analyzed using XRD method, as illustrated in Fig. 11. Comparison of XRD patterns from the same case of PC samples at 7d and 28d of curing revealed a decrease in SiO_2, Al_2O_3, and C_2S, among other substances, over time. Conversely, the presence of C-S-H, C-A-H, Aft, and other substances increased, suggesting a reaction similar to cement hydration occurred during the curing process involving the muck and FA. This resulted in the generation of hydration products like C-S-H and C-A-H, while SiO_2 and Al_2O_3 were consumed, ultimately enhancing the strength of PC. Likewise, as the true porosity increases, the micro-structure of the PC cement matrix becomes progressively looser, leading to a decrease in internal structural compactness and an increase in the number of micro-cracks and pores on the matrix surface.

4 Conclusion

(1) The control of porosity through the test mix proportion scheme is generally feasible. However, the degree of dispersion of the true porosity increases as the target porosity increases, suggesting that it becomes more challenging to control the true porosity with larger target porosity.
(2) Among the three types of SWM, muck and FA contribute to the enhancement of PC strength when the dosage is less than 10%. However, SS has a detrimental effect on the strength of PC. The dosage of muck is the primary factor influencing the strength of PC among the three types of SWM, resulting in a significant increase of 15.41% in compressive strength.
(3) The permeability coefficients of PC exhibit a pattern of initial increase followed by decrease as the dosage of all three types of SWM increases. The dosage of SS is the primary factor influencing the permeability of PC among the three types of SWM, resulting in a 39.25% increase in the permeability coefficient.
(4) The optimal PC mixture ratio scheme in this study consists of a target porosity of 25%, a water–cement ratio of 0.36, a muck content of 10%, a SS content of 10%, and a FA content of 12.5%. The corresponding measured performance indexes of PC include a true porosity of 24.67%, a compressive strength

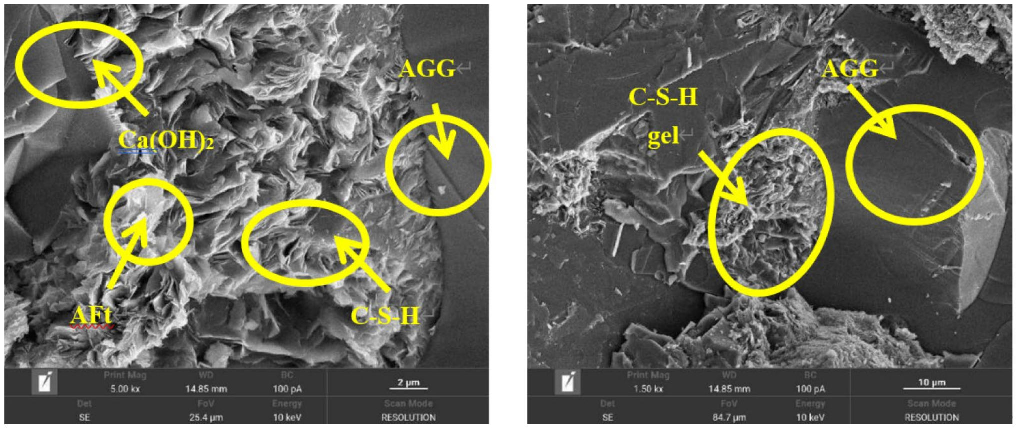

(a) SEM images of ITZ of Case 1

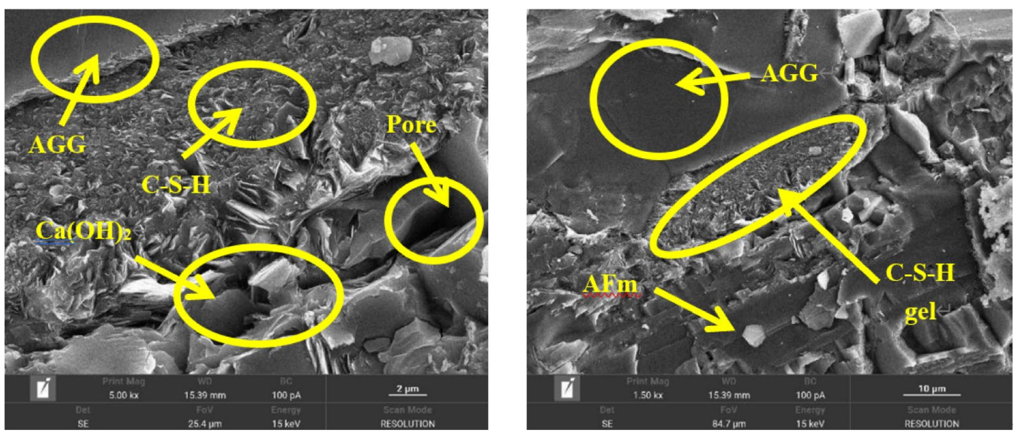

(b) SEM images of ITZ of Case 6

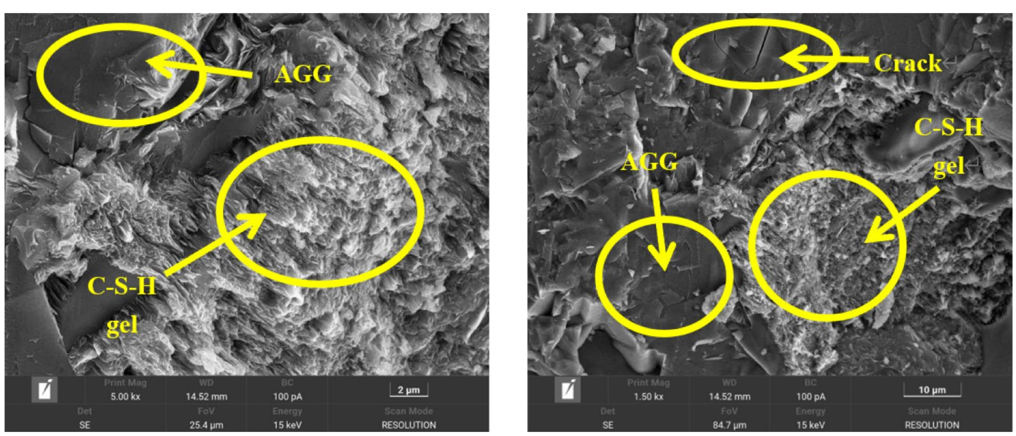

(c) SEM images of ITZ of Case 16

Fig. 9 SEM image of ITZ of PC samples.

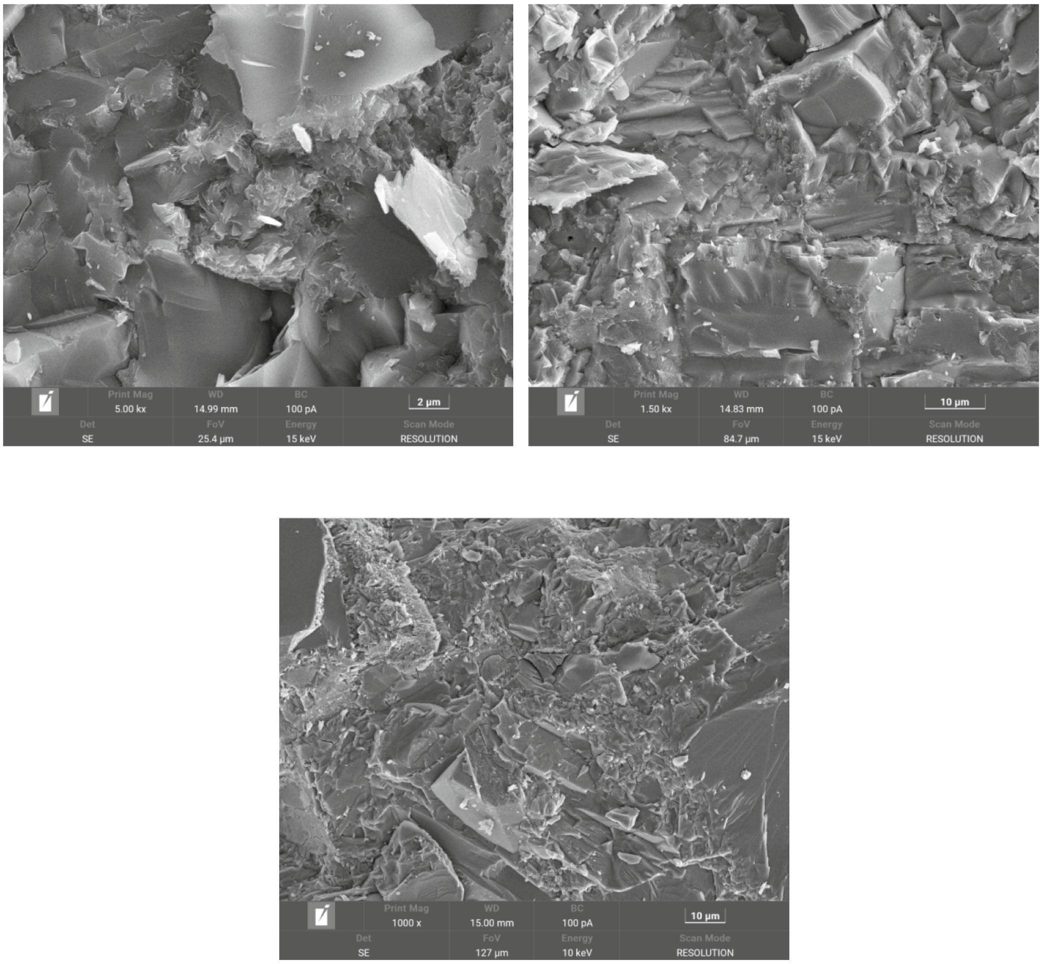

(a) SEM images of micro-structure of Case 1

Fig. 10 SEM image of micro-structure of PC samples.

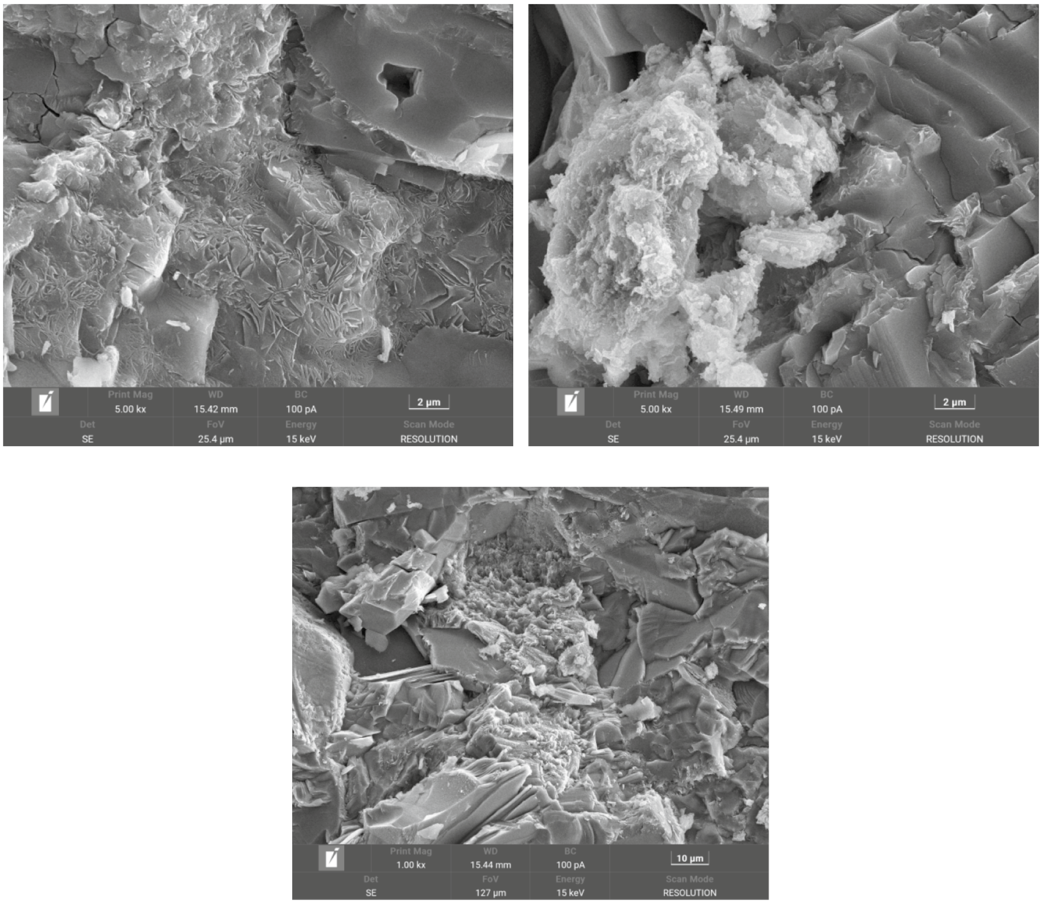

(b) SEM images of micro-structure of Case 6

Fig. 10 continued

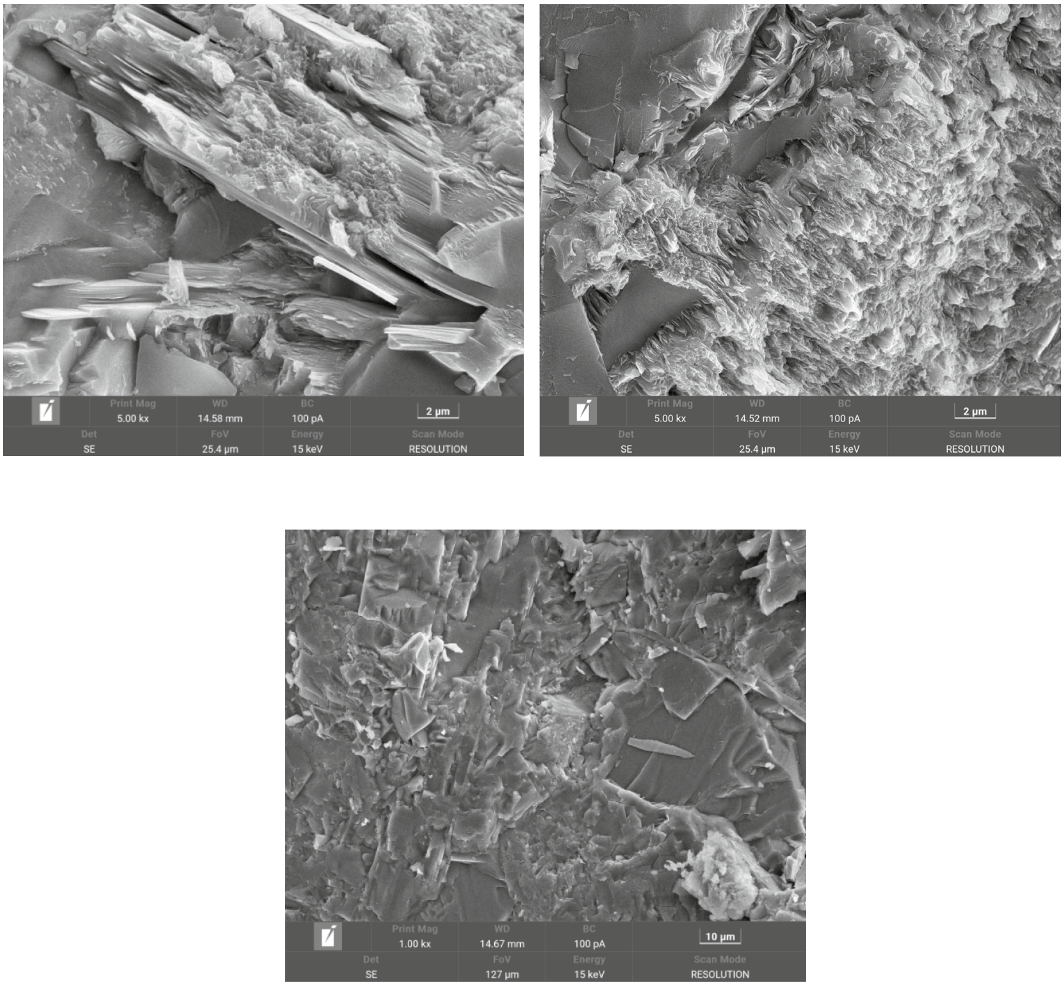

(c) SEM images of micro-structure of Case 16

Fig. 10 continued

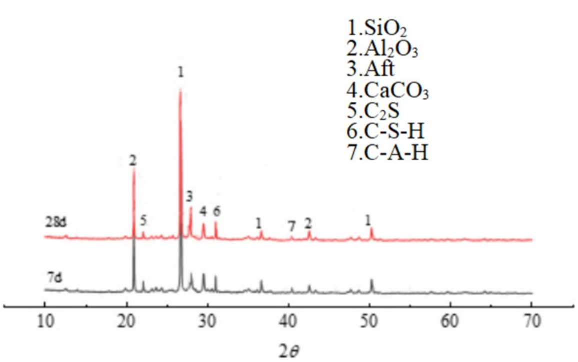

Fig. 11 Qualitative and quantitative analysis by XRD

of 15.78 MPa, and a permeability coefficient of 2.23 mm/s.

(5) In the initial hydration reaction of cement and SS, a significant quantity of $Ca(OH)_2$ is produced, resulting in the formation of an alkaline environment. This facilitates the pozzolanic reaction of active ions $[SiO_4]^{4-}$ and $[AlO_4]^{5-}$ present in muck and FA with $Ca(OH)_2$, leading to the generation of C-A-H and C-S–H which wrap around the aggregate and fill the gaps. This chemical reaction mechanism involving solid waste materials is corroborated by SEM images and XRD pattern.

(6) The active substance in SWM can react with $Ca(OH)_2$ in the reaction system, similar to the hydration reaction. The presence of $Ca(OH)_2$ nega-

tively affects the development of ITZ strength. Consequently, using SWM in the preparation of PC has a positive impact on ITZ strength.

Author contributions
Conceptualization, methodology, writing—original draft and editing were performed by Yi Li. Supervision, writing, project administration and funding acquisition were performed by Jiong Zhang. Investigation was performed by Jie Ding. Fengzhen Chen was responsible for data processing. Formal analysis was performed by Mingzhu Liu. Validation was performed by Jia Liu and Zhao Hou was responsible for writing and review.

Funding
This investigation was supported by the following funders, and their role of the funding body was declared as follows: (1) The National Natural Science Foundation of China (52078279): the design of the study. (2) The National Key R&D Program of China (2022YFB2601900): collection of data. (3) The key R&D plan of Shandong Province for major scientific and technological innovation projects (2021CXGC011205): analysis of data.

Availability of data and materials
The datasets used and analyzed during the current study are available from the corresponding author on reasonable request.

Declarations

Competing Interests
The authors declare no conflict of interest.

Received: 24 November 2023 Accepted: 5 October 2024
Published online: 20 January 2025

References

Adresi, M., Yamani, A., Karimaei Tabarestani, M., & Rooholamini, H. (2023). A comprehensive review on pervious concrete. *Construction and Building Materials, 407*, 133308. https://doi.org/10.1016/j.conbuildmat.2023.133308

Akkaya, A., & Çağatay, İH. (2021). Investigation of the density, porosity, and permeability properties of pervious concrete with different methods. *Construction and Building Materials*. https://doi.org/10.1016/j.conbuildmat.2021.123539

Basavana Gowda, S. N., Kumar Goudar, S., Thanu, H. P., & Monisha, B. (2023). Performance evaluation of alkali activated slag based recycled aggregate pervious concrete. *Materials Today Proceedings*. https://doi.org/10.1016/j.matpr.2023.04.085

Brasileiro, K. P. T. V., Nahime, B. D. O., Lima, E. C., Alves, M. M., Ferreira, W. P., Santos, I. S. D., Filho, C. P. B., & Reis, I. C. D. (2024). Influence of recycled aggregates and silica fume on the performance of pervious concrete. *J Build Eng., 82*, 108347. https://doi.org/10.1016/j.jobe.2023.108347

Bright Singh, S., Murugan, M., Chellapandian, M., Dixit, S., Bansal, S., Sunil Kumar, R. K., Gupta, M., & Maksudovna, V. K. (2023a). Effect of fly ash addition on the mechanical properties of pervious concrete. *Materials Today Proceedings*. https://doi.org/10.1016/j.matpr.2023.09.165

Bright, S. S., Murugan, M., Chellapandian, M., Dixit, S., Bansal, S., Sunil Kumar Reddy, K., Gupta, M., & Maksudovna, V. K. (2023b). Effect of fly ash addition on the mechanical properties of pervious concrete. *Materials Today Proceedings*. https://doi.org/10.1016/j.matpr.2023.09.165

Chakraborty, S., & Subramaniam, V. L. (2023). Influences of matrix strength and weak planes on fracture response of recycled aggregate concrete. *Theoretical and Applied Fracture Mechanics, 124*, 103801. https://doi.org/10.1016/j.tafmec.2023.103801

Chen, M., Zhang, Z., Deng, Q., Feng, Y., & Wang, X. (2023). Optimization of underfloor air distribution systems for data centers based on orthogonal test method: A case study. *Building and Environment, 232*, 110071. https://doi.org/10.1016/j.buildenv.2023.110071

Chockalingam, T., Vijayaprabha, C., & Leon Raj, J. (2023). Experimental study on size of aggregates, size and shape of specimens on strength characteristics of pervious concrete. *Construction and Building Materials, 385*, 131320. https://doi.org/10.1016/j.conbuildmat.2023.131320

Claudino, G. O., Rodrigues, G. G. O., Rohden, A. B., Mesquita, E. F. T., & Garcez, M. R. (2022). Mix design for pervious concrete based on the optimization of cement paste and granular skeleton to balance mechanical strength and permeability. *Construction and Building Materials, 347*, 128620. https://doi.org/10.1016/j.conbuildmat.2022.128620

Cui, X., Li, X., Du, Y., Bao, Z., Zhang, X., Hao, J., & Hu, Y. (2024). Macro-micro numerical analysis of granular materials considering principal stress rotation based on DEM simulation of dynamic hollow cylinder test. *Construction and Building Materials, 412*, 134818. https://doi.org/10.1016/j.conbuildmat.2023.134818

Cui, X., Zhang, J., Zhang, N., Gao, Z., Sui, W., & Wong, C. (2015). Improvement of permeability measurement precision of pervious concrete. *Journal of Testing and Evaluation, 43*, 20130176. https://doi.org/10.1520/JTE20130176

Dhemla, P., Somani, P., & Swami, B. L. (2023). Comparative analysis and performance of light weight concrete with varying water–cement ratio using plain and blended cement. *Materials Today Proceedings*. https://doi.org/10.1016/j.matpr.2023.07.037

Gao, W., Zhang, H., Ren, Q., Zhong, Y., & Jiang, Z. (2023). A low-carbon approach to recycling engineering muck to produce non-sintering lightweight aggregates: Physical properties, microstructure, reaction mechanism, and life cycle assessment. *Journal of Cleaner Production, 385*, 135650. https://doi.org/10.1016/j.jclepro.2022.135650

Han, X., Cui, K., Xiao, Q., Zhao, W., & Li, C. (2022). Determining the fracture properties of pervious concrete specimens with various micro-structures and geometries. *Theoretical and Applied Fracture Mechanics, 117*, 103151. https://doi.org/10.1016/j.tafmec.2021.103151

Hari, R., & K. M., M.,. (2024). Mechanical and clogging characteristics of SBR modified pervious concrete reinforced with geogrids—a functional data analysis approach. *Construction and Building Materials, 412*, 134780. https://doi.org/10.1016/j.conbuildmat.2023.134780

Hatanaka, E. R., Palamy, S., & Kurita, P. (2021). Experimental study on the porosity evaluation of pervious concrete by using ultrasonic wave testing on surfaces. *Construction & Building Materials*. https://doi.org/10.1016/j.conbuildmat.2021.123959

He, S., Jiao, C., & Li, S. (2023). Investigation of mechanical strength and permeability characteristics of pervious concrete mixed with coral aggregate and seawater. *Construction and Building Materials, 363*, 129508. https://doi.org/10.1016/j.conbuildmat.2022.129508

Lang, L., Duan, H., & Chen, B. (2019). Properties of pervious concrete made from steel slag and magnesium phosphate cement. *Construction and Building Materials, 209*, 95–104. https://doi.org/10.1016/j.conbuildmat.2019.03.123

Li, H., Yang, J., Yu, X., Zhang, Y., & Zhang, L. (2023). Permeability prediction of pervious concrete based on mix proportions and pore characteristics. *Construction and Building Materials, 395*, 132247. https://doi.org/10.1016/j.conbuildmat.2023.132247

Li, X., Wang, Z., Zhang, M., Liu, R., Wang, Z., Zhang, C., Yan, J., Liu, Y., Zhang, Z., & Wu, W. (2024). Properties of the cement containing hybrid micro-fibers and polymer latex using the orthogonal test: A comparative study of freshwater and seawater curing conditions. *Construction and Building Materials, 411*, 134661. https://doi.org/10.1016/j.conbuildmat.2023.134661

Liao, L., Wu, S., Hao, R., Zhou, Y., & Xie, P. (2023). The compressive strength and damage mechanisms of pervious concrete based on 2D mesoscale pore characteristics. *Construction and Building Materials, 386*, 131561. https://doi.org/10.1016/j.conbuildmat.2023.131561

Liu, M., Liu, Z., Wang, K., Ma, C., Zhang, H., & Zhuang, P. (2022a). Strength and deformation performances of silt-based foamed concrete under triaxial shear loading. *J Build Eng., 60*, 105237. https://doi.org/10.1016/j.jobe.2022.105237

Liu Y, Liu M, Li H, et al. Hydration kinetics of Portland cement shifting from silicate to aluminate dominance based on multi-mineral reactions and interactions[J]. Materials & Design. 2023, 233: 112228.
Liu, Y., Wan, W., Yang, F., Hu, C., Liu, Z., & Wang, F. (2022b). Performance of glass-ceramic-based lightweight aggregates manufactured from waste glass and muck. *Ceramics International, 48*, 23468–23480. https://doi.org/10.1016/j.ceramint.2022.04.342
Liu, X., Niu, D., Li, X., & Lv, Y. (2018). Effects of Ca(OH)2 – CaCO3 concentration distribution on the pH and pore structure in natural carbonated cover concrete: A case study. *Construction and Building Materials, 186*, 1276–1285. https://doi.org/10.1016/j.conbuildmat.2018.08.041
López-Carrasquillo, V., & Hwang, S. (2017). Comparative assessment of pervious concrete mixtures containing fly ash and nanomaterials for compressive strength, physical durability, permeability, water quality performance and production cost. *Construction and Building Materials, 139*, 148–158. https://doi.org/10.1016/j.conbuildmat.2017.02.052
Ministry Of Housing And Urban-Rural Development, P., 2009. Technical specification for pervious cement concrete pavement.
Nassiri S, M Rangelov, 2017. Preliminary Study to Develop Standard Acceptance Tests for Pervious Concrete.
Nazeer, M., Kapoor, K., & Singh, S. P. (2023). Strength, durability and microstructural investigations on pervious concrete made with fly ash and silica fume as supplementary cementitious materials. *J Build Eng, 69*, 106275. https://doi.org/10.1016/j.jobe.2023.106275
Nguyen, H., Tran, B., & Vu, T. (2022). Numerical approach to predict the flexural damage behavior of pervious concrete. *Case Stud Constr Mater., 16*, e946. https://doi.org/10.1016/j.cscm.2022.e00946
Oyunbileg, D., Amgalan, J., Batbaatar, T., & Temuujin, J. (2023). Evaluation of thermal and freeze-thaw resistances of the concretes with the silica fume addition at different water-cement ratio. *Case Stud Constr Mater., 19*, e2633. https://doi.org/10.1016/j.cscm.2023.e02633
Pereira Da Costa, F. B., Haselbach, L. M., & Da Silva Filho, L. C. P. (2021). Pervious concrete for desired porosity: Influence of w/c ratio and a rheology-modifying admixture. *Construction and Building Materials, 268*, 121084. https://doi.org/10.1016/j.conbuildmat.2020.121084
Ren, X., Tang, C., Xie, Y., Long, G., Ma, G., Wang, H., & Tang, Z. (2024). 3D mesoscale study on the effect of ITZ and aggregate properties on the fracture behaviors of concrete based on discrete element method. *J Build Eng., 83*, 108450. https://doi.org/10.1016/j.jobe.2024.108450
Shen, W., Liu, Y., Wu, M., Zhang, D., Du, X., Zhao, D., Xu, G., Zhang, B., & Xiong, X. (2020). Ecological carbonated steel slag pervious concrete prepared as a key material of sponge city. *Journal of Cleaner Production, 256*, 120244. https://doi.org/10.1016/j.jclepro.2020.120244
Shen, J., Xu, Q., & Liu, M. (2021). Statistical analysis of defects within concrete under elevated temperatures based on SEM image. *Construction and Building Materials, 293*, 123503. https://doi.org/10.1016/j.conbuildmat.2021.123503
Shen, W., Zhou, M., Ma, W., Hu, J., & Cai, Z. (2009). Investigation on the application of steel slag–fly ash–phosphogypsum solidified material as road base material. *Journal of Hazardous Materials, 164*, 99–104. https://doi.org/10.1016/j.jhazmat.2008.07.125
Sherwani, A. F. H., Faraj, R., Younis, K. H., & Daraei, A. (2021). Strength, abrasion resistance and permeability of artificial fly-ash aggregate pervious concrete. *Case Stud Constr Mater, 14*, e502. https://doi.org/10.1016/j.cscm.2021.e00502
Shukla, B. K., Gupta, A., Gowda, S., & Srivastav, Y. (2023). Constructing a greener future: A comprehensive review on the sustainable use of fly ash in the construction industry and beyond. *Materials Today: Proceedings*. https://doi.org/10.1016/j.matpr.2023.07.179
Teymouri, E., Wong, K. S., & Mohd Pauzi, N. N. (2023). Iron slag pervious concrete for reducing urban runoff contamination. *J Build Eng., 70*, 106221. https://doi.org/10.1016/j.jobe.2023.106221
Wang, Q., Yan, P., Yang, J., & Zhang, B. (2013). Influence of steel slag on mechanical properties and durability of concrete. *Construction and Building Materials, 47*, 1414–1420. https://doi.org/10.1016/j.conbuildmat.2013.06.044
Yao, X., Wang, H., Guan, J., Lu, M., Li, L., Zhang, M., Chen, S., & Xi, J. (2022). Statistical determination of fracture parameters of concrete with wide variation of water-cement ratio. *Mater Today Commun, 33*, 104341. https://doi.org/10.1016/j.mtcomm.2022.104341
Zhang, Q., Feng, P., Shen, X., Lu, J., Ye, S., Wang, H., Ling, T., & Ran, Q. (2023). Utilization of solid wastes to sequestrate carbon dioxide in cement-based materials and methods to improve carbonation degree: A review. *Journal of CO2 Utilization*. https://doi.org/10.1016/j.jcou.2023.102502
Zhang, G., Wang, S., Wang, B., Zhao, Y., Kang, M., & Wang, P. (2020). Properties of pervious concrete with steel slag as aggregates and different mineral admixtures as binders. *Construction and Building Materials, 257*, 119543. https://doi.org/10.1016/j.conbuildmat.2020.119543
Zhao, J., Li, Z., Wang, D., Yan, P., Luo, L., Zhang, H., Zhang, H., & Gu, X. (2023). Hydration superposition effect and mechanism of steel slag powder and granulated blast furnace slag powder. *Construction and Building Materials, 366*, 130101. https://doi.org/10.1016/j.conbuildmat.2022.130101
Zhong, R., & Wille, K. (2015). Material design and characterization of high performance pervious concrete. *Construction Building Materials., 98*, 51–60. https://doi.org/10.1016/j.conbuildmat.2015.08.027
Zhu X, Brochard L, Jiang Z, et al. Molecular simulations of premelted films between C-S-H and ice: Implication for cryo-suction in cement-based materials[J]. Cement and Concrete Research. 2023, 174: 107341.

Publisher's Note

Yi Li is a master's degree graduate with 3 years of research experience in solid waste resource utilization. He holds a master's degree and has published in the field of transportation engineering, his work has been published in the journal Materials.

Jiong Zhang is a professor with more than 10 years of research experience in pervious concrete. He holds a PhD and has published extensively in the field of pervious concrete, with his work appearing in journals such as Journal of Cleaner Production.

Jie Ding is a master's degree graduate with 3 years of research experience in solid waste resource utilization. She holds a master's degree and has published in the field of transportation engineering, her work has been published in the journal Materials.

Feng-zhen Chen is a engineer with many years of research experience in resource reuse of sewage sludge. He holds a master's degree.

Ming-zhu Liu is an engineer with many years of research experience in resource reuse of sewage sludge. He holds a master's degree.

Jia Liu is a master's degree graduate with 2 years of research experience in solid waste resource utilization. He has published in the field of transportation engineering, his work has been published in the journal Materials.

Zhao Hou is a master's degree graduate with 2 years of research experience in solid waste resource utilization. He has published in the field of transportation engineering, his work has been published in the journal Materials.